Numerical Simulations on Two Nonlinear Biharmonic Evolution Equations

Ming-Jun Lai *, Chun Liu †, and Paul Wenston**

Abstract

We numerically simulate the following two nonlinear evolution equations with a fourth order (biharmonic) leading term:

$$-\Delta^2 u - \frac{1}{\epsilon^2}(|u|^2 - 1)u = u_t \qquad \text{in } \Omega \subset \mathbf{R}^2 \text{ or } \mathbf{R}^3$$

and

$$-\Delta^2 u + \frac{1}{\epsilon^2}\nabla \cdot ((|\nabla u|^2 - 1)\nabla u) = u_t \qquad \text{in } \Omega \subset \mathbf{R}^2 \text{ or } \mathbf{R}^3$$

with an initial value and a Dirichlet boundary conditions. We use a bivariate spline space like finite element method to solve these equations. We discuss the convergence of our numerical scheme and present several numerical experiments under different boundary conditions and different domains in the bivariate setting.

AMS 2000 Mathematics Subject Classifications: 35J35, 35K55, 65M12, 65M60
Keywords and Phrases: Nonlinear Biharmonic evolution equations, Ginzburg-Landau type equations, Bivariate Spline Method

§1. Introduction

In this paper, we are interested in the numerical behavior of the following two biharmonic equations

$$\begin{cases} -\Delta^2 u - \frac{1}{\epsilon^2}(|u|^2 - 1)u = u_t, & \text{in } \Omega \subset \mathbf{R}^2 \text{ or } \mathbf{R}^3 \\ u(x,0) = u_0(x), & x \in \Omega \\ u(x,t) = u_1(x) & x \in \partial\Omega \\ \frac{\partial u}{\partial n}(x,t) = u_2(x) & x \in \partial\Omega \end{cases} \tag{1.1}$$

* Department of Mathematics, University of Georgia, Athens, GA 30602. This author is supported by the National Science Foundation under Grant #DMS-9870178. His email address is mjlai@math.uga.edu.

† Department of Mathematics, Pennsylvania State University, University Park, PA 16802. His email address is liu@math.psu.edu.

** Department of Mathematics, University of Georgia, Athens, GA 30602. His email address is paul@math.uga.edu.

and

$$
\begin{cases}
-\Delta^2 u + \dfrac{1}{\epsilon^2}\nabla\cdot((|\nabla u|^2-1)\nabla u) = u_t, & \text{in } \Omega\subset \mathbf{R}^2 \text{ or } \mathbf{R}^3 \\
u(x,0) = u_0(x), & x\Omega \\
u(x,t) = u_1(x) & x\in\partial\Omega \\
\frac{\partial u}{\partial n}(x,t) = u_2(x) & x\in\partial\Omega,
\end{cases} \tag{1.2}
$$

where Ω is a bounded domain in $\mathbf{R}^2$ or $\mathbf{R}^3$ and n is the outward normal of the boundary $\partial\Omega$.

Equation (1.1) may be regarded as the gradient flow of the following energy functional:

$$
E(u) := \frac{1}{2}\int_\Omega \left(|\Delta u|^2 + \frac{1}{2\epsilon^2}(|u|^2-1)^2\right) dx \tag{1.3}
$$

in the class

$$
\mathcal{C} = \{u\in H^2(\Omega),\ u\big|_{\partial\Omega} = u_1, \frac{\partial}{\partial n}u\big|_{\partial\Omega} = u_2\}. \tag{1.4}
$$

Similarly, equation (1.2) is the gradient flow of the energy functional

$$
E(u) := \frac{1}{2}\int_\Omega \left(|\Delta u|^2 + \frac{1}{2\epsilon^2}(|\nabla u|^2-1)^2\right) dx \tag{1.5}
$$

in the class (1.4).

The understanding of the above two equations were originally motivated by our earlier study in the smectic liquid crystals (cf. [LLW03]). In that paper, the existence, uniqueness and stability of the solutions of both equations were established. In particular, for both equations, one of the important issues is to study the asymptotic behavior as $\epsilon\to 0$. However, little is known about the variational problem involving the second order derivative term as those in (1.3) and (1.5). From the analysis point of view, one main difficulty is the lack of the maximum principle.

In [LLW03], we used a special bivariate spline space in our proofs of the global existence of the weak solutions. We recall the weak formulation for (1.1): find $u\in L_2(0,T,H_0^2(\Omega))$ such that

$$
\begin{aligned}
\int_\Omega u_t v dx + \int_\Omega \Delta u\Delta v dx + \frac{1}{\epsilon^2}\int_\Omega (u^2-1)uv dx \\
= \int_\Omega f(u)v dx
\end{aligned} \tag{1.6}
$$

for all $v\in H_0^2(\Omega)$. The weak formulation for (1.2) is as follows: Find $u\in L_2(0,T,H_0^2(\Omega))$ such that

$$
\begin{aligned}
\int_\Omega u_t v dx + \int_\Omega \left[\Delta u\Delta v + \frac{1}{\varepsilon^2}(|\nabla u|^2-1)\nabla u\nabla v\right] dx \\
= \int_\Omega f(u)v dx
\end{aligned} \tag{1.7}
$$

for all $v \in H_0^2(\Omega)$. Here, we have already substracted a biharmonic function with the original boundary conditions in (1.1) and (1.2). See [LLW03] for a detailed treatment and the compatiblity of the boundary conditions.

We used the bivariate spline space $S_{3r}^r(\diamondsuit)$ as finite dimensional approximation space in our Galerkin's procedure. The spline space mentioned above is defined as

$$S_{3r}^r(\diamondsuit) = \{S \in C^r(\Omega) : \quad s|_t \in \mathbf{P}_{3r}, \forall t \in \diamondsuit\},$$

where $\mathbf{P}_{3r}$ is the space of all polynomials of degree $\leq 3r$ and $\diamondsuit$ is a triangulated quadrangulation of the domain $\Omega \subset \mathbf{R}^2$ which is obtained from a nondegenerate quadrangulation $\heartsuit$ of Ω by adding two diagonals of each quadrilateral in $\heartsuit$ (cf. [Lai and Schumaker99]). Such a special triangulation is general enough to partition any polygonal domains.

We will show the convergence of the spline solution to the weak solution of the equations (1.1) and (1.2) in §2 and §3, respectively. We explore the asymptotic behavior of the numerical solutions as time $t \longrightarrow \infty$ and $\epsilon \longrightarrow 0$. We encountered many interesting phenomena indicating the possibility of the nonuniqueness of the solutions to the steady state equations (1.1) and (1.2) as ϵ very small. That is, there could be many critical points for (1.3) and (1.5) or there are many paths leading to the minimizer.

§2. Numerical Analysis of Equation (1.1)

In this section, we will present numerical analysis and simulation of the spline solutions to both the steady state equation (2.1) below and the time dependent equation (1.1). We will Newton's method to solve the nonlinear equations (2.1) and Crank-Nicolson's method in time steps for (1.1). Find $u \in V \subset H_0^2(\Omega)$ such that

$$a_2(u, v) + b(u, u, v) - \langle f(u), v\rangle - \langle g, v\rangle = 0 \tag{2.1}$$

for all $v \subset V \subset H_0^2(\Omega)$, where

$$a_2(\phi, \psi) = \int_\Omega \Delta\phi\Delta\psi dx$$

and

$$b(\theta, \phi, \psi) = \frac{1}{\epsilon^2}\int_\Omega (|\theta|^2 - 1)\phi\psi dx.$$

The stationary problem of equation (1.1) can be converted into (2.1) for a certain $f(u)$ (cf. [LLW03]).

Let $V = S_{3r}^r(\diamondsuit) \bigcap H_0^2(\Omega)$ be a spline subspace in $H_0^2(\Omega)$. We may absorb $\langle g, v\rangle$ into $\langle f(u), v\rangle$ and follow the same arguments of Theorem 2.3 in [LLW03] to have

Theorem 2.1. *For any $\varepsilon > 0$, there exists a weak solution $S_u \in V$ satisfying (2.1).*

Alternatively we may use the Brouwer fixed point theorem to prove Theorem 2.1. (cf. [Lai and Wenston'98] for such kind of proof for the nonlinear biharmonic equation associated with the Navier-Stokes equations.)

Note that the proof of Lemma 2.5 in [LLW03] can be used to prove the boundedness of S_u. That is,

Lemma 2.1. *Let S_u be a weak solution satisfying (2.1) with $V = S_{3r}^r(\Delta) \bigcap H_0^2(\Omega)$. Then*

$$\int_\Omega |\Delta S_u|^2 dx \le C(\epsilon)|\Omega|.$$

Also, the proof of Theorem 2.4 in [LLW03] yields the following

Theorem 2.2. *If ϵ is not very small, then the weak solution $S_u \in V$ is unique.*

We now see how close S_u is to the weak solution u. Consider

$$\epsilon^2 a_2(u - S_u, u - S_u) = \epsilon^2 a_2(u - S_u, u - S) + \epsilon^2 a_2(u - S_u, S - S_u)$$

where S is a spline function in $S_{3r}^r(\Delta) \bigcap H_0^2(\Omega)$.

Note that we have

$$\begin{aligned}
&a_2(u - S_u, S - S_u) \\
=&b(S_u, S_u, S - S_u) - b(u, u, S - S_u) + \langle f(S_u) - f(u), S - S_u\rangle \\
=&b(S_u, S_u, u - S_u) + b(S_u, S_u, S - u) - b(u, u, u - S_u) \\
&+ b(u, u, u - S) - \frac{3}{\epsilon^2}\langle \phi(S_u + u)(S_u - u), S - S_u\rangle \\
&- \frac{3}{\epsilon^2}\langle \phi(S_u - u), S - S_u\rangle
\end{aligned}$$

For $b(S_u, S_u, S - u) + b(u, u, u - S)$, we have, by using a well-known inequality

$$\int_\Omega f^4 dx \le 2 \int_\Omega f^2 dx \int_\Omega |\nabla f|^2 dx$$

and by Poincaré's inequality,

$$\begin{aligned}
&|b(S_u, S_u, u - S) - b(u, u, u - S)| \\
&\le |b(S_u, u - S_u, u - s)| + |b(u, u, u - S) - b(S_u, u, u - S)| \\
&\le \frac{1}{\epsilon^2} C_1(|S_u|_{1,\Omega}^2 + 1)|S_u - u|_{1,\Omega}|u - S|_{1,|\Omega} \\
&\quad + \frac{1}{\epsilon^2} C_2 |S_u - u|_{1,\Omega}(|S_u|_{1,\Omega} + |u|_{1,\Omega})|u|_{1,\Omega}|u - S|_{1,\Omega} \\
&\le C(\epsilon, K, |\Omega|)|S_u - u|_{2,\Omega}|u - S|_{1,\Omega},
\end{aligned}$$

where $|\cdot|_{k,\Omega}$ is the usual semi norm of $H^k(\Omega)$ and $C(\epsilon, K, |\Omega|)$ is a constant. Here, we have used Lemma 2.1 and Theorem 2.5 in [LLW03].

For $b(S_u, S_u, u - S_u) - b(u, u, u - S_u)$, we have

$$\begin{aligned}
&\epsilon^2(b(S_u, S_u, u - S_u) - b(u, u, u - S_u)) \\
&= -\frac{1}{4}\int_\Omega |S_u - u|^4 dx - \frac{3}{4}\int_\Omega |u^2 - S_u^2|^2 dx + \int_\Omega |S_u - u|^2 dx.
\end{aligned}$$

For $\frac{1}{\epsilon^2}\langle\phi(S_u+u)(S_u-u),S-S_u\rangle+\frac{1}{\epsilon^2}\langle\phi(S_u-u),S-S_u\rangle$, we have,

$$\begin{aligned}
&|\langle\phi(S_u+u)(S_u-u),S-S_u\rangle+\langle\phi(S_u-u),S-S_u\rangle|\\
&\le|\langle\phi(S_u+u)(S_u-u),u-S_u\rangle+\langle\phi(S_u-u),u-S_u\rangle|\\
&\quad+|\langle\phi(S_u+u)(S_u-u),S-u\rangle+\langle\phi(S_u-u),S-u\rangle|\\
&\le\sqrt{2}Km(|S_u|_{0,\Omega}+|u|_{0\Omega})|u-S_u|^2_{1,\Omega}+\sqrt{2}mK^2|u-S_u|^2_{1,\Omega}\\
&\quad+\sqrt{2}K^2m(|S_u|_{0,\Omega}+|u|_{0,\Omega})|u-S_u|_{1,\Omega}|u-S|_{1,\Omega}\\
&\quad+\sqrt{2}K^2m|u-S_u|_{1,\Omega}|u-S|_{1,\Omega}\\
&\le C_3(m,K,\epsilon,|\Omega|)|u-S_u|^2_{2,\Omega}\\
&\quad+C_3(m,K,\epsilon,|\Omega|)|u-S_u|_{2,\Omega}|u-S|_{2,\Omega}
\end{aligned}$$

for a constant C_3 which is dependent on m,K,ϵ and $|\Omega|$, where K is the Poincaré constant. We now summarize the above discussion to have

$$\begin{aligned}
&\epsilon^2a_2(u-S_u,u-S_u)+\frac{1}{4}\int_\Omega|S_u-u|^4dx+\frac{3}{4}\int_\Omega|u^2-S_u^2|^2dx\\
&=\epsilon^2a_2(u-S_u,u-S)+\int_\Omega|S_u-u|^2dx\\
&\quad+\epsilon^2b(S_u,S_u,S-u)+\epsilon^2b(u,u,u-S)\\
&\quad-3\langle\phi(S_u^2-u^2),S-S_u\rangle-3\langle\phi(S_u-u),S-S_u\rangle\\
&\le\epsilon^2|u-S_u|_{2,\Omega}|u-S|_{2,\Omega}+K^4|u-S_u|^2_{2,\Omega}\\
&\quad+C(\epsilon,K,|\Omega|)|u-S_u|_{2,\Omega}|u-S|_{2,\Omega}\\
&\quad+C_3(m,K,\epsilon|\Omega|)|u-S_u|_{2,\Omega}\\
&\quad+C_3(m,K,\epsilon|\Omega|)|u-S_u|_{2,\Omega}|u-S|_{2,\Omega}.
\end{aligned}$$

Thus, we have

$$\begin{aligned}
&(\epsilon^2-K^4-C_3(m,\epsilon,K,|\Omega|))|u-S_u|_{2,\Omega}\\
\le&(\epsilon^2+C(\epsilon,K,|\Omega|)+C_3(m,K,\epsilon,|\Omega|))|u-S|_{2,\Omega}.
\end{aligned}$$

That is, $|u-S_u|_{2,\Omega}\le\alpha|u-S|_{2,\Omega}$ for any $S\in S_3^1(\diamondsuit)\cap H_0^2(\Omega)$, where constant $\alpha=(\epsilon^2+C(\epsilon,K,|\Omega|)+C_3(m,K,\epsilon|\Omega|))/(\epsilon^2-K^4-C(m,\epsilon,K,|\Omega|))$. By using the spline approximation property (c.f. Theorem 1.1 in [Lai and Schumaker'99]), we complete the proof of the following

Theorem 2.3. *Suppose that ϵ is not very small. Suppose that $\phi\in H^k(\Omega)$ with $k\ge3$. Then the bivariate spline solution S_u approximates the weak solution u and satisfies*

$$|S_u-u|_{2,\Omega}\le C|\Diamond\!\!\!\!\!\!\diamond|^{k-2}|\phi|_{k,\Omega}.$$

Next we discuss the implementation of bivariate spline spaces to numerically solve both the equation (1.1) and its steady state equation (2.1). We apply bivariate spline space

$S_3^1(\diamondsuit)$ to discretize the space variables of the equations (1.1) using Galerkins's method and use Crank-Nicolson's method to discretize the time variable of the equations (1.1). For each step we employ the Newton method to iterate the nonlinear term in (1.1). We set the error between iterations to be 10^{-8} for a stopping criterion. For the time dependent problem (1.1), we use the solution at $t = t_i$ to be an initial guess for the solution for $t = t_{i+1}$ and then apply the Newton method. More precisely, our numerical scheme for (2.1) is

1) Start with $S_{u,0} \in S_3^1(\diamondsuit)$ which is the numerical solution of a biharmonic equation:

$$\begin{cases} \int_\Omega \Delta S_{u,0} \Delta v dx = \int_\Omega g v dx, \quad \text{for all } v \in S_3^1(\diamondsuit) \cap H_0^2(\Omega) \\ u\big|_{\partial\Omega} = u_1(x), \\ \frac{\partial}{\partial n} u\big|_{\partial\Omega} = u_2(x) \end{cases}$$

2) For $k = 1, 2, 3, \cdots$, use Newton's method to solve $S_{u,k} \in S_3^1(\diamondsuit)$ satisfying

$$\begin{cases} \int_\Omega \Delta S_{u,k} \Delta v dx + \int_\Omega f(S_{u,k}) v dx = \int_\Omega g v dx \\ u\big|_{\partial\Omega} = u_1(x), \\ \frac{\partial}{\partial n} u\big|_{\partial\Omega} = u_2(x). \end{cases}$$

3) Letting $S_{u,k} = \sum_{i=1}^{N} c_{i,k}\phi_i$, if $\|\{c_{i,k}\} - \{c_{i,k-1}\}\|_{\ell^\infty} < 10^{-8}$, we stop the Newton iteration in 2) and use $S_{u,k}$ as the spline approximation of the weak solution of (2.1).

Finally, we present some numerical experiments with the equations (1.1) and (2.1). We did the following two sets of numerical experiments. First, we test if our programs work correctly by inputing the programs the right-hand side and boundary conditions computed from a known test function u, computing a numerical approximation S_u, and comparing the maximum errors between u and S_u for several refinements of a underlying quadrangulation of a given domain. We did such a test for several functions over different domains. We tabulate some experimental results below in Tables 4.1–4.6. In the following Tables 4.1–4.2, we numerically solve equation (2.1) with known exact solutions $u(x, y) = x^4 + y^4$ and $u(x, y) = \sin(xy)$. We list the maximum errors of the numerical solutions against the exact solutions evaluated over 101×101 points equally-spaced over $[0, 1] \times [0, 1]$ for different values ϵ.

Table 2.1. The maximum errors of numerical solutions of (2.1) against the exact solution $u(x, y) = x^4 + y^4$.

matrix size	$\epsilon = 1$	$\epsilon = \sqrt{0.1}$	$\epsilon = \sqrt{0.01}$	$\epsilon = \sqrt{0.001}$	$\epsilon = \sqrt{0.0005}$
155×155	7.316×10^{-4}	8.392×10^{-4}	1.998×10^{-3}	3.137×10^{-2}	7.936×10^{-1}
547×547	6.983×10^{-5}	7.640×10^{-5}	1.465×10^{-4}	2.086×10^{-3}	9.888×10^{-1}
2051×2051	6.082×10^{-6}	6.490×10^{-6}	1.083×10^{-5}	1.313×10^{-4}	9.965×10^{-1}
7939×7939	4.811×10^{-7}	5.065×10^{-7}	7.785×10^{-7}	8.314×10^{-6}	9.970×10^{-1}

Table 2.2. The maximum errors of numerical solutions of (2.1) against the exact solution $u(x, y) = \sin(xy)$.

matrix size	$\epsilon = 1$	$\epsilon = \sqrt{0.1}$	$\epsilon = \sqrt{0.01}$	$\epsilon = \sqrt{0.001}$	$\epsilon = \sqrt{0.0005}$
155×155	9.796×10^{-5}	9.768×10^{-5}	9.843×10^{-5}	3.014×10^{-3}	1.035×10^{0}
547×547	1.053×10^{-5}	1.059×10^{-5}	1.112×10^{-5}	2.876×10^{-5}	1.161×10^{0}
2051×2051	8.287×10^{-7}	8.313×10^{-7}	8.749×10^{-7}	2.090×10^{-6}	1.165×10^{0}
7939×7939	5.688×10^{-8}	5.709×10^{-8}	5.925×10^{-8}	1.304×10^{-7}	1.165×10^{0}

When $\epsilon = \sqrt{0.0005}$, our numerical experiments confirm the nonuniqueness of the solution of (2.1). That is, starting from the spline solution of the biharmonic equation, the iterations converge. However, they converge to a different solution than the exact solution. That is why the errors in Tables 4.1–2 do not decrease as the refinement level increases. In Figures 4.1–4.2, we show graphs of two numerical solutions of (2.1) associated with the same boundary conditions.

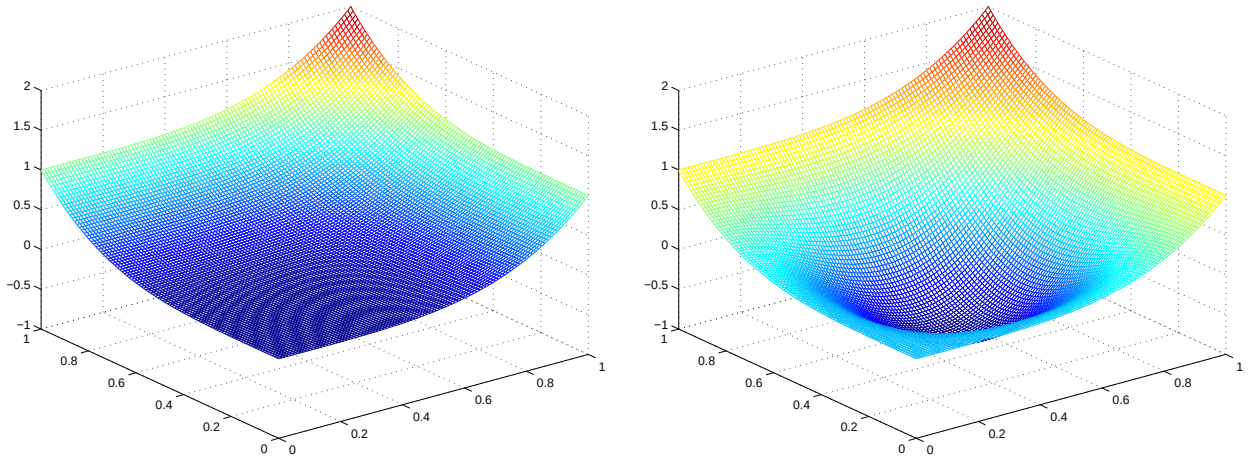

Fig. 2.1 Two numerical solutions of the equation (2.1) with the same boundary conditions and $\epsilon = \sqrt{0.0005}$.

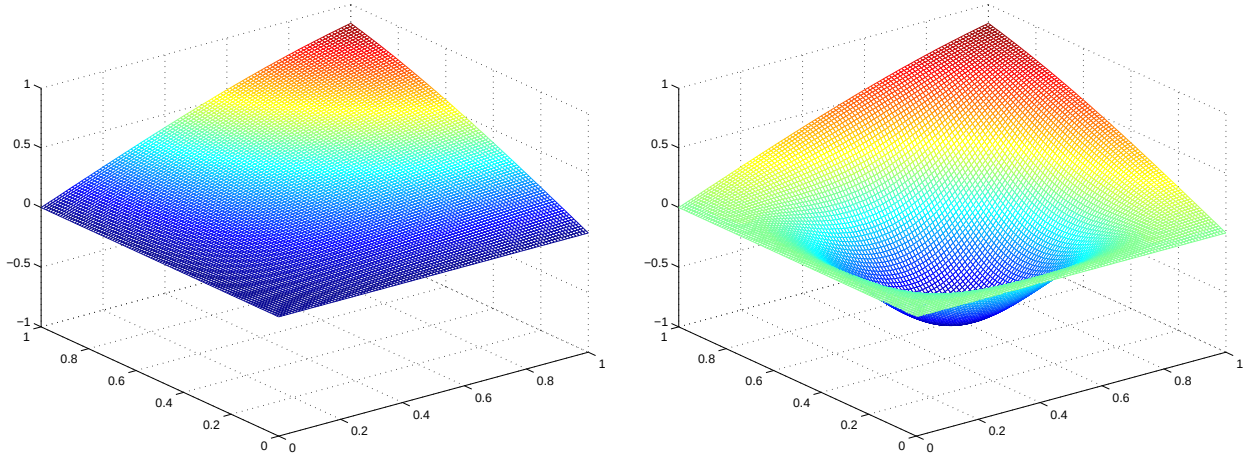

Fig. 4.2 Another two numerical solutions of the equation (2.1) with the same boundary conditions. Here, $\epsilon = \sqrt{0.0005}$.

Secondly, we test if the numerical solutions of (1.1) converge to the solution of the steady state equation (2.1). We input the programs the right-hand sides and boundary conditions computed from a known test function u, input the programs with various initial values, compute the numerical solutions S_u at $t = 1, 2, 5$ and 10, and then compare the maximum errors between u and S_u. We list the maximum errors for various initial values, different times $t = 1, 2, 5$ and 10 and various values ϵ.

Table 2.3. The maximum errors of numerical solutions of (1.1) with boundary conditions obtained from $u(x, y) = x^4 + y^4$ and initial value $u(x, y) = (x^4 + y^4)(1 - \sin(\pi x)\sin(\pi y))$ against the exact solution $u(x, y) = x^4 + y^4$.

time	$\epsilon = 1$	$\epsilon = \sqrt{0.1}$	$\epsilon = \sqrt{0.01}$	$\epsilon = \sqrt{0.001}$	$\epsilon = \sqrt{0.0005}$
$t = 1$	8.812×10^{-2}	8.852×10^{-2}	9.235×10^{-2}	1.022×10^{-1}	7.364×10^{-1}
$t = 2$	3.407×10^{-2}	3.417×10^{-2}	3.507×10^{-2}	5.197×10^{-2}	7.831×10^{-1}
$t = 5$	8.882×10^{-3}	9.009×10^{-3}	1.034×10^{-2}	3.973×10^{-2}	7.930×10^{-1}
$t = 10$	6.941×10^{-3}	6.898×10^{-3}	6.455×10^{-3}	3.393×10^{-2}	7.941×10^{-1}

Table 2.4. The maximum errors of numerical solutions of (1.1) with boundary conditions obtained from $u(x, y) = x^4 + y^4$ and initial value $u(x, y) = 1$ against the exact solution $u(x, y) = x^4 + y^4$.

time	$\epsilon = 1$	$\epsilon = \sqrt{0.1}$	$\epsilon = \sqrt{0.01}$	$\epsilon = \sqrt{0.001}$	$\epsilon = \sqrt{0.0005}$
$t = 1$	2.735×10^{-2}	2.679×10^{-2}	2.206×10^{-2}	5.887×10^{-2}	7.815×10^{-1}
$t = 2$	8.326×10^{-3}	8.321×10^{-3}	8.352×10^{-3}	4.160×10^{-2}	8.130×10^{-1}
$t = 5$	3.280×10^{-3}	3.313×10^{-3}	3.807×10^{-3}	2.936×10^{-3}	8.121×10^{-1}
$t = 10$	2.443×10^{-3}	2.495×10^{-3}	3.092×10^{-3}	2.687×10^{-2}	8.045×10^{-1}

Table 2.5. The maximum errors of numerical solutions of (1.1) with boundary conditions obtained from $u(x, y) = \sin(xy)$ and initial value $u(x, y) = \sin(xy)(1 - \sin(\pi x)\sin(\pi y))$ against the exact solution $u(x, y) = \sin(xy)$.

time	$\epsilon = 1$	$\epsilon = \sqrt{0.1}$	$\epsilon = \sqrt{0.01}$	$\epsilon = \sqrt{0.001}$	$\epsilon = \sqrt{0.0005}$
$t = 1$	5.052×10^{-2}	5.009×10^{-2}	4.580×10^{-2}	2.133×10^{-2}	9.818×10^{-1}
$t = 2$	3.157×10^{-2}	3.140×10^{-2}	2.975×10^{-2}	2.026×10^{-2}	1.017×10^{0}
$t = 5$	1.322×10^{-2}	1.319×10^{-2}	1.288×10^{-2}	9.750×10^{-3}	1.034×10^{0}
$t = 10$	4.258×10^{-3}	4.249×10^{-3}	4.163×10^{-3}	4.048×10^{-3}	1.035×10^{0}

Table 2.6. The maximum errors of numerical solutions of (1.1) with boundary conditions obtained from $u(x, y) = \sin(xy)$ and initial value $u(x, y) = 1$ against the exact solution $u(x, y) = \sin(xy)$.

time	$\epsilon = 1$	$\epsilon = \sqrt{0.1}$	$\epsilon = \sqrt{0.01}$	$\epsilon = \sqrt{0.001}$	$\epsilon = \sqrt{0.0005}$
$t = 1$	9.943×10^{-3}	9.381×10^{-3}	5.409×10^{-3}	4.890×10^{-2}	9.619×10^{-1}
$t = 2$	3.327×10^{-3}	3.323×10^{-3}	3.406×10^{-3}	2.836×10^{-2}	1.025×10^{0}
$t = 5$	1.294×10^{-3}	1.305×10^{-3}	1.440×10^{-3}	1.412×10^{-2}	1.048×10^{0}
$t = 10$	7.292×10^{-4}	7.197×10^{-4}	6.233×10^{-4}	6.721×10^{-3}	1.044×10^{0}

From Tables 2.3–2.6, we see that for $\epsilon > \sqrt{0.0005}$, the numerical solutions of (1.1) converges to the exact solution of the steady state equation (2.1) as t increases. This verifies Theorem 2.4. However, when $\epsilon = \sqrt{0.0005}$, the numerical solution of (1.1) in Table 2.3–2.6 does not converge to $x^4 + y^4$ and $\sin(xy)$. Instead, it converges to the other numerical solution of (2.1) as shown in the right graph of Fig. 2.1 and Fig. 2.2. We have evaluated their energy functional at the solutions. The energy of the solutions in the right graph of Figs 2.1 and 2.2 is smaller than the energy of the exact solutions.

§3. Numerical Simulation of the Equation (1.2)

In this section, we study the numerical solution to both the steady state equation (3.1) below and time dependent equation corresponding to (3.1).

$$\begin{cases} \Delta^2 u + \frac{1}{\epsilon^2}\nabla\cdot(|\nabla u|^2 - 1)\nabla u) = g, \quad \text{in } \Omega \\ u\big|_{\partial\Omega} = u_1(x), \\ \frac{\partial}{\partial n}u\big|_{\partial\Omega} = u_2(x). \end{cases} \tag{3.1}$$

The study is similar to §2 although it is more complicated. Let us outline the main steps and ingredients.

We first express the equation (3.1) in a weak formulation. Find $u \in V \subset H_0^2(\Omega)$ such that

$$a_2(u,v) + b(u,u,v) - \langle f(u), v\rangle - \langle g, v\rangle = 0 \tag{3.1}$$

for all $v \subset V \subset H_0^2(\Omega)$, where

$$b(\theta,\phi,\psi) = \frac{1}{\epsilon^2}\int_\Omega (|\nabla\theta|^2 - 1)\nabla\phi\cdot\nabla\psi dx$$

and

$$\begin{aligned} -\epsilon^2\langle f(u), v\rangle = &\int_\Omega |\nabla u|^2\nabla\phi\cdot\nabla v dx + \\ &2\int_\Omega \nabla u\cdot\nabla\phi\nabla u\cdot\nabla v dx + 2\int_\Omega \nabla u\cdot\nabla\phi\nabla\phi\cdot\nabla v dx \\ &+\int_\Omega |\nabla\phi|^2\nabla u\cdot\nabla v dx - \int_\Omega \nabla\phi\cdot\nabla v dx + \int_\Omega |\nabla\phi|^2\nabla\phi\cdot\nabla v dx \end{aligned}$$

with ϕ being the biharmonic function with the original boundary conditions.

Let $V = S_{3r}^r(\Delta\!\!\!\!\Delta)\bigcap H_0^2(\Omega)$ be a spline subspace in $H_0^2(\Omega)$ as before. We may use the Brouwer fixed point theorem to prove Theorem 3.1 (cf. [Lai and Wenston'00] for such kind of proof for the nonlinear biharmonic equation associated with Navier-Stokes equations).

Theorem 3.1. *For any $\varepsilon > 0$, there exists a weak solution $S_u \in V$ satisfying (5.1).*

Note that the proof of Lemma 3.4 in [LLW03] can be used to prove the boundedness of S_u. That is,

Lemma 3.1. *Let S_u be a weak solution satisfying (3.1) with $V = S_{3r}^r(\Delta\!\!\!\!\Delta)\bigcap H_0^2(\Omega)$. Then*

$$\int_\Omega |\Delta S_u|^2 dx \le C(\epsilon)|\Omega|.$$

Similar to Theorem 3.4 in [LLW03], we have

Theorem 3.2. *If ϵ is not very small, then the weak solution S_u is unique.*

We next study the approximation of S_u to u. Consider

$$\epsilon^2 a_2(u - S_u, u - S_u) = \epsilon^2 a_2(u - S_u, u - S) + \epsilon^2 a_2(u - S_u, S - S_u)$$

for any spline function $S \in V$. Note that we have

$$\begin{aligned}
&a_2(u - S_u, S - S_u)\\
=&b(S_u, S_u, S - S_u) - b(u, u, S - S_u) + \langle f(S_u) - f(u), S - S_u\rangle\\
=&b(S_u, S_u, u - S_u) + b(S_u, S_u, S - u) - b(u, u, u - S_u) + b(u, u, u - S)\\
&+ \frac{1}{\epsilon^2}\langle(|\nabla S_u|^2 - |\nabla u|^2), \nabla\phi\cdot\nabla(S - S_u)\rangle + \frac{1}{\epsilon^2}\langle|\nabla\phi|^2, \nabla(S_u - u)\cdot\nabla(S - S_u)\rangle\\
&+ \frac{2}{\epsilon^2}\langle\nabla(S_u - u)\cdot\nabla\phi, \nabla\phi\cdot\nabla(S - S_u)\rangle + \frac{2}{\epsilon^2}\langle\nabla(S_u - u)\cdot\nabla\phi, \nabla S_u\cdot\nabla(S - S_u)\rangle\\
&+ \frac{2}{\epsilon^2}\langle\nabla(S_u - u)\cdot\nabla(S - S_u), \nabla\phi\cdot\nabla u\rangle.
\end{aligned}$$

The last four terms in the above can be bounded by $C(m, \epsilon, K, |\Omega|)|S - S_u|_{2,\Omega}|S_u - u|_{2,\Omega}$ as in §4, where $C(m, \epsilon, K, |\Omega|)$ is a positive constant. Also, the first four terms on the right-hand side in the above can be treated exactly as in §4 with $\nabla\phi$ in place of ϕ. Therefore we should get the same result. That is,

Theorem 3.3. *Suppose that ϵ is not very small. Suppose that $u \in H^k(\Omega)$ with $k \geq 3$. Then the bivariate spline solution S_u satisfying (3.1) approximates the weak solution u such that*

$$|S_u - u|_{2,\Omega} \leq C|\Delta|^{k-2}|u|_{k,\Omega}.$$

Finally we discuss the implementation of $S_3^1(\Delta)$ to numerically solve both the equation (1.2) and its steady state equation (3.1). We use $S_3^1(\Delta)$ to discretize the space variables of the equations (1.2) and (3.1) by Galerkins's method and use Crank-Nicolson's method to discretize the time variable of the equations (1.2). For each step we employ the Newton method to iterate the nonlinear term in (1.2) and (3.1). We set the error between iterations to be 10^{-8} for a stopping criterion. For the time dependent problem (1.2), we use the solution at $t = t_i$ to be an initial guess for the solution for $t = t_{i+1}$.

Our numerical scheme for (1.2) is

1) Start with $S_{u,0} \in S_3^1(\Delta)$ which is the numerical solution of a biharmonic equation:

$$\begin{cases} \int_\Omega \Delta S_{u,0}\Delta v dx = \int_\Omega g v dx, \quad \text{for all } v \in S_3^1(\Delta) \cap H_0^2(\Omega)\\ u\big|_{\partial\Omega} = u_1(x),\\ \frac{\partial}{\partial n}u\big|_{\partial\Omega} = u_2(x) \end{cases}$$

2) For $k = 1, \cdots,$, solve $S_{u,k} \in S_3^1(\Delta)$ satisfying

$$\begin{cases} \int_\Omega \Delta S_{u,k}\Delta v dx = \int_\Omega g v dx - \int_\Omega f(S_{u,k-1})\cdot\nabla v dx,\\ u\big|_{\partial\Omega} = u_1(x),\\ \frac{\partial}{\partial n}u\big|_{\partial\Omega} = u_2(x) \end{cases}$$

3) Letting $S_{u,k} = \sum_{i=1}^{N} c_{i,k}\phi_i$, if $\|\{c_{i,k}\} - \{c_{i,k-1}\}\| < 10^{-8}$ we stop the above iteration.

Let us explain the computation of the nonlinear terms in (3.1) in detail. Let S_u be an approximation of u in the spline space $S_3^1(\Diamond)$. Note that $f(u,\epsilon)$ is a function of $\frac{\partial}{\partial x}u$ and $\frac{\partial}{\partial y}u$. Thus, we write $f(u,\epsilon) = [f_1(\frac{\partial}{\partial x}u, \frac{\partial}{\partial x}u)), f_2(\frac{\partial}{\partial x}u, \frac{\partial}{\partial y}u)]$ and we approximate f_1 and f_2 by quadratic finite elements associated with the underlying triangulation $\Diamond$. That is, letting $W = \{w_i, i = 1, \cdots, M\}$ be the collection of all vertices of $\Diamond$ and the midpoints of all edges of $\Diamond$,

$$f_1(\frac{\partial}{\partial x}u, \frac{\partial}{\partial y}u) = \sum_{i=1}^{M} f_1(\frac{\partial}{\partial x}u(w_i), \frac{\partial}{\partial y}u(w_i))h_i(x,y)$$

and similar for f_2, where h_i is the continuous quadratic finite element basis function satisfying $h_i(w_j) = \delta_{ij}$ for all $i, j = 1, \cdots, M$.

We numerically solve equation (3.1) with known exact solutions $u(x,y) = x^4 + y^4$ and $u(x,y) = \sin(xy)$. In the following Tables 3.1–3.2, we list the maximum errors of the numerical solutions against the exact solutions evaluated over 101×101 points equally-spaced over $[0,1] \times [0,1]$ for different values ϵ.

Table 3.1. The maximum errors of numerical solutions of (3.1) against the exact solution $u(x,y) = x^4 + y^4$.

matrix size	$\epsilon = \sqrt{0.1}$	$\epsilon = \sqrt{0.01}$	$\epsilon = \sqrt{0.001}$	$\epsilon = \sqrt{0.0001}$
155×155	6.7765×10^{-3}	1.7776×10^{-2}	2.2802×10^{-1}	2.4646×10^{-1}
547×547	3.0644×10^{-4}	5.6518×10^{-4}	3.1132×10^{-1}	3.4315×10^{-1}
2051×2051	1.6614×10^{-5}	4.0444×10^{-5}	3.1602×10^{-1}	3.6134×10^{-1}
7939×7939	1.0178×10^{-6}	2.5822×10^{-6}	3.1752×10^{-1}	3.6581×10^{-1}

Table 3.2. The maximum errors of numerical solutions of (1.9)′ against the exact solution $u(x,y) = \sin(xy)$.

matrix size	$\epsilon = \sqrt{0.1}$	$\epsilon = \sqrt{0.01}$	$\epsilon = \sqrt{0.001}$	$\epsilon = \sqrt{0.0001}$
155×155	7.8411×10^{-4}	5.9811×10^{-3}	1.5842×10^{-1}	3.6648×10^{-1}
547×547	1.9821×10^{-4}	1.8209×10^{-3}	2.1533×10^{-1}	3.1509×10^{-1}
2051×2051	5.0229×10^{-5}	4.6871×10^{-4}	3.0612×10^{-1}	2.8182×10^{-1}
7939×7939	1.2432×10^{-5}	1.1810×10^{-4}	3.1199×10^{-1}	2.6908×10^{-1}

From Tables 3.1 and 3.2, we see that for $\epsilon > \sqrt{0.001}$, the numerical solutions of (3.1) converges to the exact solution as the refinement level increases. However, when

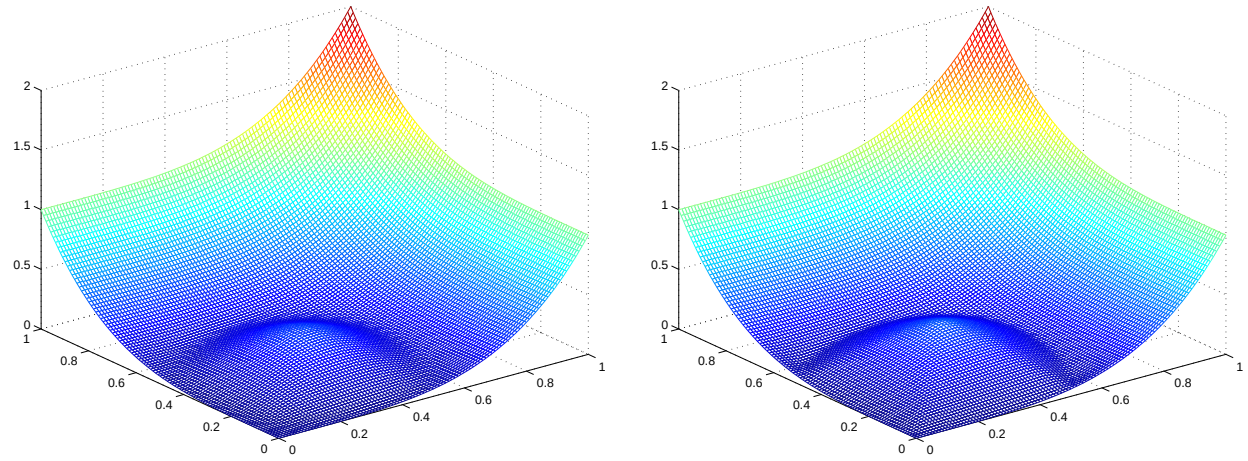

Fig. 3.1. Numerical solution of equation $(1.9)'$ with $\epsilon = \sqrt{0.001}$ and $\epsilon = \sqrt{0.0001}$

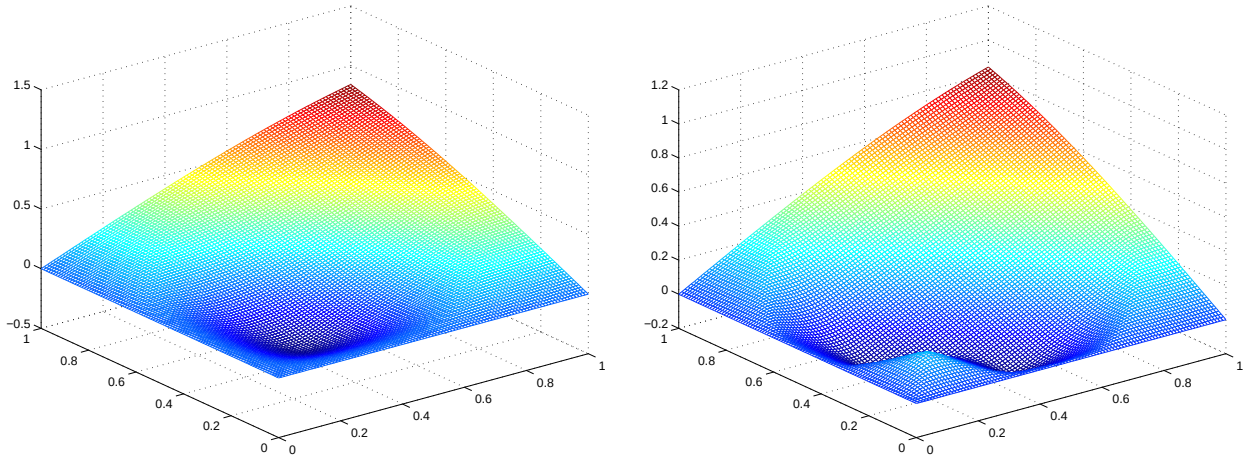

Fig. 3.2. Numerical solution of equation $(1.9)'$ with $\epsilon = \sqrt{0.001}$ and $\epsilon = \sqrt{0.0001}$

$\epsilon \leq \sqrt{0.001}$, the numerical solution of (3.1) in Tables 3.1 and 3.2 does not converge to x^4+y^4 and $\sin(xy)$. Instead, it converges to the other numerical solution of (3.1) as shown in Fig. 3.1 and Fig. 3.2. We have computed their energy functional. The energy of the solutions in the Figs 3.1–3.2 are almost the same as the energy of the exact solutions x^4+y^4 and $\sin(xy)$, respectively.

We have also applied the continuation or homotopy technique to solve the equation. That is, we started with the numerical solution associated with $\epsilon = 1$ as an initial value to compute the solution associated with $\epsilon = \sqrt{0.1}$. Then using the solution with $\epsilon = \sqrt{0.1}$ as an initial value, we compute the numerical solution associated with $\epsilon = \sqrt{0.01}$. And so on. We were able to find a very good approximation of the exact solution for $\epsilon = \sqrt{0.001}$ and $\epsilon = \sqrt{0.0001}$ for all refinements of underlying quadrangulations.

References

[1] S. Allen and J. Cahn, A microscopic theory for the antiphase boundary motion and its application to antiphase domain coarsening, Acta Metallurgica, 27 (1979), pp. 1085–1095.

[2] S. Angenet and M. Gurtin, Multiphase thermo-mechanics with interfacial structure.

Evolution of an isothermal interface, Acta Rational Mech. Math. Anal. 108(1989), pp. 333-391.

[3] L. Bronsard and R. Kohn. Motion by mean curvature as the singular limit of Ginsburg-Landau dynamics, J.D.H. Eqs. 20(1991), pp. 214–137.

[4] M. Carme Calderer, C. Liu and K. Voss, Radial configurations of smectic A materials and focal conics, Submitted. 1997.

[5] M. Carme Calderer, C. Liu and Karl Voss, Smectic A Liquid Crystal Configurations with Interface Defects Submitted to Physica D (1998).

[6] Du, Q., M. D. Gunzburger, J. S. Peterson, Analysis and approximation of the Ginsburg Landau model of superconductivity, SIAM Review, 34(1992) pp. 54–81.

[7] W. E, Nonlinear Continuum Theory of Smectic-A Liquid Crystals, Preprint, 1997.

[8] P. Grisvard, *Elliptic Problems on Nonsmooth Domains*, Pitman, Boston, 1985.

[9] W.M. Jin, Singular Perturbations, Fold Energies and Micromagnetics, Ph. D. thesis, Courant Institute, 1997.

[10] D. Kinderlehrer and C. Liu, Revisiting the Focal Conic Structures in Smectic A. *Proc. Symposium on Elasticity to honor Professor J. L. Ericksen 1996, ASME Mechanics and Materials Conference.*

[11] R. Kohn, A singular perturbed variational problem describing thin film blisters, IMA workshop, Feb. 5–9, 1996.

[12] M. J. Lai and L. L. Schumaker, On the approximation power of splines on triangulated quadrangulations, SIAM J. Num. Anal., **36**(1999), pp. 143–159.

[13] M. J. Lai, C. Liu and P. Wenston, On two nonlinear biharmonic evolution equations: existence, uniqueness and stability, to appear in Applicable Analysis, 2003.

[14] M. J. Lai and P. Wenston, Bivariate spline method for the steady state Navier-Stokes equations, Numerical Methods for PDE, 16(2000), pp. 147–183.

[15] M. Ortiz and G. Gioia, 1994, The morphology and folding patterns of buckling-driven thin-film blisters, J. Mech. Phys. Solids, **42**(1994), pp. 531–559.

[16] J. Rubinstein, P. Sternberg and J. Keller. Fast reaction, slow diffusion and curve shortening. SIAM J. Appl. Math., 49(1989), pp. 116-133.

[17] R. Kohn and P. Sternberg, Local minimizers and singular perturbations, Proc. Roy. Soc. Edinburgh Sect. A **111**(1989), pp. 69–84.

[18] P. Sternberg, The effect of a singular perturbation on nonconvex variational problems, Arch. Rational. Mech. Anal, 101(1988), pp. 109–160.